4192 *Chem. Mater.* **2009,** *21,* 4192–4202
DOI:10.1021/cm900721r

CHEMISTRY OF MATERIALS
Article

Photochemical Synthesis of Water-Soluble Gold Nanorods: The Role of Silver in Assisting Anisotropic Growth

Tiziana Placido,[†,‡] Roberto Comparelli,*[,†] Francesco Giannici,[§] P. Davide Cozzoli,[⊥,∥] Giancarlo Capitani,[○,#] Marinella Striccoli,[†] Angela Agostiano,[†,‡] and M. Lucia Curri[†]

[†]*National Research Council CNR-IPCF Sez. Bari, c/o Dip. Chimica, Via Orabona 4, Bari, I-70126, Italy,* [‡]*Università degli Studi di Bari, Dipartimento di Chimica, Via Orabona 4, Bari, I-70126, Italy,* [§]*Università di Palermo, Dip. di Chimica Inorganica e Analitica, 90128 Palermo, Italy,* [⊥]*Scuola Superiore ISUFI, Università del Salento, Distretto Technologico ISUFI, via per Arnesano km 5, 73100 Lecce, Italy,* [∥]*National Nanotechnology Laboratory of CNR-INFM, Unità di Ricerca IIT, Distretto Tecnologico ISUFI, via per Arnesano km 5, 73100 Lecce, Italy, and* [○]*Università degli Studi di Bari, Dip. Geomineralogico,70126 bari, Italy.* [#] *Present address: Università di Milano Bicocca, Dip. di Geologia e Geotecnologie, P.za della Scienza 4, I-20126, Milano, Italy*

Received March 13, 2009. Revised Manuscript Received June 1, 2009

The role of Ag^+ ions in the ultraviolet-driven photochemical synthesis of Au nanorods (NRs) in aqueous surfactant mixtures has been investigated in order to elucidate the mechanism that drives anisotropic nanoparticle growth. The samples, grown in the presence of varying amounts of Ag^+ ions for scheduled irradiation times, have been characterized by ultraviolet−visible−near infrared (UV−vis−NIR) absorption spectroscopy, analytical transmission electron microscopy (ATEM), inductively coupled plasma atomic emission spectroscopy (ICP-AES), and extended X-ray absorption fine structure (EXAFS) measurements. Moreover, the time evolution of size and shape distribution has been investigated by statistical analysis of the relevant TEM data. EXAFS measurements at the Ag K-edge have unambiguously disclosed the presence of Ag species in the final product, identifying their chemical state as well as the most probable lattice environment around them with a reasonably high level of confidence. The extensive sample knowledge gained by the combination of spectroscopic, structural, and morphological measurements has provided reliable information regarding the most relevant processes underlying the Ag^+-assisted formation of Au NRs by the photochemical route. An induction period prior to occurrence of fast nanoparticle nucleation has been identified, which has been correlated to the slow accumulation of a critical concentration of Au(I)−surfactant species from reduction of their Au(III) parent precursors. The role played by Ag in directing Au growth toward the formation of NRs has been clarified through demonstration of preferential adsorption of zerovalent Ag species on {110} facets of the growing Au nanoparticles, which can be therefore responsible for restricting crystal development along the relevant crystallographic directions.

Introduction

Over the past decade, reports on the synthesis and use of Au nanoparticles (NPs) as promising nanomaterials for photonic, catalytic, sensing, and biomedical technologies have proliferated due to their unusual dimensionality-related physical−chemical behavior, which remarkably diverges from that exhibited by their bulk material counterpart.[1−5]

Especially, the optical properties of nanosized Au in the visible and near-infrared region of the spectrum, which are indeed strongly dependent on size, shape, aggregation state, and local environment, have been the subject of both fundamental and application-oriented studies.[1−3] A typical example is represented by the peculiar optical response of anisotropically shaped NPs.[6] It is well-known that the surface plasmon resonance (SPR) absorption of Au nanorods (NRs) is featured by two bands, corresponding to the collective oscillations of the free conduction band electrons along the longitudinal and transverse axes of the NRs, respectively. The transverse mode shows a resonance at around 520 nm, which is coincident with the SPR band of spherical particles of similar diameter, while the spectral position of the longitudinal mode is progressively red-shifted as the aspect ratio (defined as the long to short axis ratio) of NRs increases.[7]

Because of the relevance of nanosized Au in many technological fields, great attention has been devoted to

*Corresponding author. E-mail: r.comparelli@ba.ipcf.cnr.it.

(1) Daniel, M. C.; Astruc, D. *Chem. Rev.* **2004**, *104*, 293.
(2) Law, M.; Sirbuly, D. J.; Johnson, J. C.; Goldberger, J.; Saykally, R. J.; Yang, P. *Science* **2004**, *305*, 1269.
(3) Maier, S. A.; Brongersma, M. L.; Kik, P. G.; Meltzer, S.; Requicha, A. A. G.; Atwater, H. A. *Adv. Mater.* **2001**, *13*, 1501.
(4) Maier, S. A.; Kik, P. G.; Atwater, H. A.; Meltzer, S.; Harel, E.; Koel, B. E.; Requicha, A. A. G. *Nat. Mater.* **2003**, *2*, 229.
(5) Rosi, N. L.; Mirkin, C. A. *Chem. Rev.* **2005**, *105*, 1547.
(6) Nehl, C. L.; Hafner, J. H. *J. Mater. Chem.* **2008**, *18*, 2415.
(7) Link, S.; El-Sayed, M. A. *J. Phys. Chem. B* **1999**, *103*, 8410.

 Published on Web 08/28/2009 © 2009 American Chemical Society

develop synthetic routes for producing metal NPs in tailored size and shape regimes.[8] As of today, it appears clear that future cost-effective exploitation of such appealing class of nanomaterials will ultimately rely on the availability of NPs with programmable geometric parameters in large-scale quantities.

Metal NRs and nanowires have been synthesized by using a variety of techniques, including membrane templating,[9] photochemical,[10] seed-catalyzed,[11] seedless,[12] combined chemical−photochemical,[13] microwave-assisted,[14] and electrochemical[15] approaches. Among these methods, colloidal seed-mediated routes in aqueous media have been among the most widely investigated strategies, since they allow the gram-scale preparation of metallic NPs at nearly room temperature.[11,16−21] However, so far, the formation mechanism of anisotropic shaped NPs has not been fully understood, due to the intrinsic complexity of the reaction systems devised for the synthesis, on one side, and to the largely different effects of the numerous experimental parameters involved therein, on the other side. In fact, it has now been demonstrated that even minor changes in the content, the chemical nature, and the purity of any of the involved reactants (e.g., Au salt precursors, additives, reducing agents, surfactants), and in the size, age, as well as surface coating of the catalyst seeds, can lead to dramatic alterations in the size−morphological features of the NRs eventually achievable.[22] In recently proposed protocols, Au ion reduction has been accomplished in complex mixtures of surfactants, whereby the presence of a suitable cosurfactant species has been found to guarantee the formation of more flexible micellar templates.[16] To this aim, several cosurfactants have been tested, among which benzyldimethylammonium chloride (BDAC),[16] Tween 20 and Triton X-100,[23] Pluronic F-127,[24] tetraoctylammonium bromide (TOAB),[10,25] tetradodecylammonium bromide (TDDAB),[15,26,27] and tetrahexylammonium bromide (THAB) are some examples.[13] In spite of significant advances in the development of increasingly refined colloidal routes, the poor reproducibility in product preparation yet remains one of the major unsolved issues in the synthesis of anisotropic Au NPs.[22]

On the basis of a seed-mediated procedure, Au NRs have been prepared, albeit with modest yield, with aspect ratios up to 25.[28] More recently, this method has been modified by the introduction of Ag^+ ions to controllably drive anisotropic growth, which has led to the production of shorter Au NRs with uniform aspect ratio tunable in between ∼2 and ∼5 in nearly quantitative yield.[16,29,30]

Water-soluble Au nanospheres and NRs can be also prepared by one-pot seedless photochemical growth in the presence of selected surfactants.[26] Such route represents one of the most straightforward approaches to obtain Au NRs, as it can be carried out under experimental conditions easy to implement without the complication of preparing catalyst seeds in a separate step. In addition, NP growth is allowed to proceed rather slowly, thereby permitting a detailed monitoring of the reaction progress (e.g., by spectroscopic and transmission electron microscopy analyses). As already observed in the seed-mediated synthesis, also in the photochemical approach it has been noted that small, calibrated amounts of Ag^+ ions are critical to promote the formation of NRs with controllable aspect ratios instead of spherical NPs.[26] However the role of such Ag^+ additive in the growth mechanism of Au NRs is still mostly unclear. Although the $[Au^{3+}]$:$[Ag^+]$ molar ratio realized in the reaction environment has been correlated to the shape of the resulting Au nanostructures, whereby the growth of {100} facets has been found to be somehow favored by the presence of Ag^+ ions;[26,31] nevertheless, to the best of our knowledge, no ultimate demonstration for the fate of Ag^+ employed as shape anisotropy promoter both in the photochemical and in the seed-mediated approaches has been reported.

Here, we report on the investigation on the role of Ag^+ ions in the UV-driven photochemical synthesis of Au NPs in a micellar template realized in a mixture of surfactants (namely cetyltrimethylammonium bromide and tetrakis (decyl)ammoniumbromide). We performed a systematic study on the effect of Ag^+ ion concentration and of the irradiation time in order to elucidate the mechanism that generates anisotropic NPs rather than nanospheres. The samples have been characterized by combining ultraviolet−visible−near infrared (UV−vis−NIR) absorption spectroscopy, analytical transmission electron microscopy (TEM), inductively coupled plasma atomic emission spectroscopy (ICP-AES), and extended X-ray absorption fine structure (EXAFS) spectroscopy measurements. Moreover, the temporal evolution of the size and shape distribution of the growing NPs has also been investigated by statistical analysis of TEM

(8) Tao, A. R.; Habas, S.; Yang, P. *Small* **2008**, *4*, 310.
(9) van der Zande, B. M. I.; Bohmer, M. R.; Fokkink, L. G. J.; Schonenberger, C. *J. Phys. Chem. B* **1997**, *101*, 852.
(10) Miranda, O. R.; Ahmadi, T. S. *J. Phys. Chem. B* **2005**, *109*, 15724.
(11) Murphy, C. J.; Jana, N. R. *Adv. Mater.* **2002**, *14*, 80.
(12) Jana, N. R. *Small* **2005**, *1*, 875.
(13) Niidome, Y.; Nishioka, K.; Kawasaki, H.; Yamada, S. *Colloid Surf. A−Physicochem. Eng. Asp.* **2005**, *257−258*, 161.
(14) Zhu, Y.-J.; Hu, X.-L. *Chem. Lett.* **2003**, *32*, 1140.
(15) Yu, Y. Y.; Chang, S. S.; Lee, C. L.; Wang, C. R. C. *J. Phys. Chem. B* **1997**, *101*, 6661.
(16) Nikoobakht, B.; El-Sayed, M. A. *Chem. Mater.* **2003**, *15*, 1957.
(17) Jana, N. R.; Gearheart, L.; Murphy, C. J. *J. Phys. Chem. B* **2001**, *105*, 4065.
(18) Pérez-Juste, J.; Liz-Marzán, L. M.; Carnie, S.; Chan, D. Y. C.; Mulvaney, P. *Adv. Funct. Mater.* **2004**, *14*, 571.
(19) Wang, Z. L.; Mohamed, M. B.; Link, S.; El-Sayed, M. A. *Surf. Sci.* **1999**, *440*, L809.
(20) Gai, P. L.; Harmer, M. A. *Nano Lett.* **2002**, *2*, 771.
(21) Wei, Z.; Zamborini, F. P. *Langmuir* **2004**, *20*, 11301.
(22) Jiang, X. C.; Brioude, A.; Pileni, M. P. *Colloid Surf. A−Physicochem. Eng. Asp.* **2006**, *277*, 201.
(23) Yong, K.-T.; Sahoo, Y.; Swihart, M.; Schneeberger, P.; Prasad, P. *Top. Catal.* **2008**, *47*, 49.
(24) Iqbal, M.; Chung, Y.-I.; Tae, G. *J. Mater. Chem.* **2007**, *17*, 335.
(25) Miranda, O. R.; Dollahon, N. R.; Ahmadi, T. S. *Cryst. Growth Des.* **2006**, *6*, 2747.
(26) Kim, F.; Song, J. H.; Yang, P. *J. Am. Chem. Soc.* **2002**, *124*, 14316.
(27) Chang, S. S.; Shih, C. W.; Chen, C. D.; Lai, W. C.; Wang, C. R. C. *Langmuir* **1999**, *15*, 701.
(28) Gao, J.; Bender, C. M.; Murphy, C. J. *Langmuir* **2003**, *19*, 9065.
(29) Gou, L.; Murphy, C. J. *Chem. Mater.* **2005**, *17*, 3668.
(30) Sau, T. K.; Murphy, C. J. *J. Am. Chem. Soc.* **2004**, *126*, 8648.
(31) Liu, M. Z.; Guyot-Sionnest, P. *J. Phys. Chem. B* **2005**, *109*, 22192.

Table 1. List of Samples and Preparation Conditions

sample	[Au]:[Ag] molar ratio
Au_no_Ag	without Ag^+ added
Au_60	60:1
Au_30	30:1
Au_20	20:1
Au_15	15:1

data. Especially, EXAFS analyses at Ag K-edges have been demonstrated to be a valuable tool for revealing the presence of Ag in the final NP product, its chemical state, and the chemical environment around it with a reasonably high degree of confidence. Overall, the obtained results have allowed us to prove the relevance of the presence of Ag^+ ions in assisting Au NR formation and to demonstrate their ultimate role in activating anisotropic growth pathways.

Experimental Section

Materials. Hydrogen tetrachloroaurate(III) trihydrate ($HAuCl_4 \cdot 3H_2O$ ≥99.9%), cetyltrimethylammonium bromide (CTAB), and silver nitrate ($AgNO_3$ 99.9999%) have been purchased from Aldrich. Tetrakis (decyl)ammoniumbromide (TDAB ≥99.9%), cyclohexane (≥99.5%) have been obtained from Fluka. Acetone (99.8%) has been purchased from Carlo Erba. Stock ion solutions have been prepared using deionized water (Millipore milli-Q Gradient A-10 system).

General Protocol for the Photochemical Synthesis of Au Nanorods (NRs). In a typical synthesis, a fixed amount of $HAuCl_4$ precursor (0.006 mmol) has been dissolved in water in the presence of 60 μL of acetone (the radical initiator),[10,32] 45 μL of cyclohexane (able to influence the micelle morphology),[27] 0.24 mmol of CTAB and 0.0045 mmol of TDAB as surfactant and cosurfactant, respectively. Five different set of samples have been prepared at increasing concentration of $AgNO_3$ added to the growth solution described above, so as to vary the Au:Ag molar ratio in the range 60:1−15:1 (Table 1). The as-prepared mixtures have been exposed to the UV light produced by a 8 W Hg lamp (Model ENF-280 C/FE at 50 Hz frequency from Spectroline; $\lambda \geq$ 254 nm) and kept at a constant temperature of 19.5 ± 0.1 °C. At scheduled reaction time (7, 12, 17, 21, 26, 44, 63, and 88 h) aliquots have been withdrawn from the reaction vessel for optical, morphological, chemical, and structural investigations. The formed Au NPs have been collected by centrifuging the samples at 30 000 rpm (ultracentrifuge Optima L-60; Beckman) for 15 min at 25 °C. Prior to analysis, the NPs have been further purified upon repeated cycles of dissolution in water and ultracentrifugation to wash out surfactant residuals and adsorbed reaction byproducts.

Sample Characterization. *UV−Visible Spectroscopy.* UV−vis absorption spectra of solutions of the as-prepared NPs and of the residual reaction mixture after NP extraction have been recorded using a Varian Cary 5000 UV−vis−NIR scanning spectrophotometer in the 300−800 nm range. The samples have been typically diluted with Millipore water (1:50) so as to realize an absorbance value lower than ∼1 at the transverse SPR band peak.

Inductively Coupled Plasma Atomic Emission Spectroscopy (*ICP-AES*). Sample aliquots withdrawn at the scheduled irradiation times have been centrifuged and the concentrations of Au and Ag in both the supernatant and the separated powders have been analyzed by ICP-AES with an Optima Model 3000 Instrument (Perkin-Elmer). The samples for ICP-AES analyses have been digested in concentrated $HCl:HNO_3$ mixtures.

Transmission Electron Microscopy (*TEM*). TEM investigations have been performed by both a Jeol JEM-1011 microscope operating at 100 kV, and a Jeol JEM-2010 microscope, operating at 200 kV. The latter has been equipped with an energy dispersive spectrometer (EDS) for chemical analysis. The specimens have been prepared by depositing a few drops of aqueous NP dispersions onto a carbon-coated copper grid and then allowing the solvent to evaporate.

A systematic statistical analysis of NP size/shape distributions has been performed on the basis of low-magnification TEM images with the help of Axio Vision software. At least 200 NPs have been counted for each sample. Convergent beam electron diffraction (CBED) experiments have been performed on single NPs to gain an insight into their crystal growth anisotropy. In particular, the facet of the particle lying on the supporting carbon film has been identified from the direction of observation (the pole of that facet), which, in turn, has been retrieved upon indexing the electron diffraction pattern. The latter, being integral with the particle image, has also allowed identification of the side facets (through their poles on the diffraction pattern) and of the lattice elongation direction.

X-ray Absorption Spectroscopy (*XAS*). XAS measurements at Ag K-edge (25.5 keV) have been performed in fluorescence mode at the GILDA BM8 Beamline of the ESRF facility (Grenoble-France), on samples prepared in different conditions. Due to the high dilution (approximately 10^{-4} M) of the target photoabsorber (i.e., Ag species) in the investigated samples, in order to separate the Ag fluorescence signal from the Au fluorescence and scattered radiation, the spectra have been recorded with an energy-resolving 13-elements Ge detector, and the monochromator has been operated in sagittal focusing mode to achieve maximum flux on the sample. All spectra have been collected at room temperature and analyzed using Viper software.[33]

Results

In the UV-assisted photochemical synthesis of Au NRs investigated, the presence of Ag^+ ions at low and controllable concentration levels in the growing $HAuCl_4$-loaded surfactant environment is critical for directing the growth of Au NPs toward anisotropic shapes.[26] Therefore, here, in order to elucidate the role of Ag^+ ion additives in this system, various sets of samples have been prepared and investigated as a function of the Ag content in the growing reaction mixture and of the irradiation time.

The experiments have been carried out in a mixture of surfactants (CTAB and TDAB), in the presence of tiny amounts of acetone and cyclohexane. The latter two ingredients have been found essential for triggering NP formation. On one side, in the absence of acetone, neither Au nor Ag NPs can be generated, irrespective of the relative reactant proportions used and of the irradiation time considered.[32] This evidence preliminarily suggests that acetone is indeed required for metal ion reduction to take place. On the other side, syntheses carried out without cyclohexane lead to the uncontrollable formation of

(32) Nishioka, K.; Niidome, Y.; Yamada, S. *Langmuir* **2007**, *23*, 10353.

(33) Klementev, K. V. *J. Phys. D−Appl. Phys.* **2001**, *34*, 209.

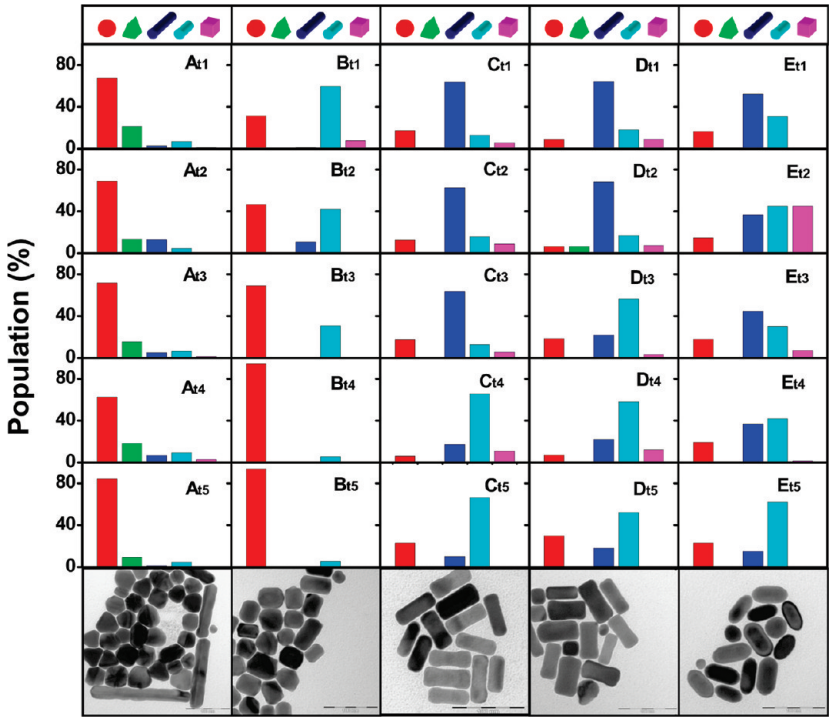

Figure 1. Statistical analysis of Au NP shape evolution as a function of the irradiation time The sample sets correspond to: (A) Au_no_Ag, (B) Au_60, (C) Au_30, (D) Au_20, (E) Au_15 series, respectively (cf. Table 1). The irradiation times at which the aliquots have been extracted are denoted in the relevant panels as follows: (t1) 17, (t2) 21, (t3) 26, (t4) 63, (t5) 88 h. The colors in the histograms are related to the main types of shapes observed, as indicated by the legend in the top part of the figure. In the bottom part of the figure, representative TEM images of NPs obtained after irradiating for 17 h in the respective cases, are shown (scale bar 100 nm).

anisotropic shaped Au NPs that exhibit exceedingly broad distributions of sizes and aspect ratios (data not reported).

The whole set of experiments for each sample series, summarized in Table 1, has been monitored by following the time evolution of different parameters. An estimation of the changes in the degree of NP shape anisotropy has been inferred by monitoring the evolution of optical absorbance spectra, whereby shifts in the spectral position of the longitudinal SPR band (if any appears) reflect the growth of NPs with increasingly higher aspect ratios (ARs). The variations in the average NP shape and dimensions have been evaluated by statistical analysis of TEM micrographs. In addition, the amounts of Au and Ag elements in the as-collected NPs, as well as in the corresponding supernatants (i.e., the liquid reaction mixture after NP extraction) have been followed by ICP-AES analyses performed on aliquots withdrawn during the synthesis. At each sampling time scheduled, these data have provided information regarding the relative level of consumption of Ag and Au precursors along the course of NP growth.

Additionally, the chemical composition of individual NPs grown in different conditions and with different shapes has been analyzed by EDS performed in a TEM microscope. The preferential growth direction of the NPs has been determined by combining CBED and TEM imaging on several nano-objects. Finally, the chemical state of Ag and its local lattice environment in the final NP product has been investigated by XAS at Ag K-edge.

In the following, the dependence of the shape and AR of the formed Au NPs on the nominal Ag^+ content will be examined in detail for the prepared samples.

Spectroscopic and Morphological Characterization. *Evolution of NP Shapes.* Figure 1 summarizes the results of the statistical shape distribution analyses for samples grown in different conditions as a function of the irradiation time, "*t*" (cf. Table 1). In the absence of Ag^+ ions (Au_no_Ag series,) a predominance of isotropic NPs (spheres + polyhedrons >85%) with respect to anisotropic NPs (triangular prisms + NRs < 10−12%; Figure 1A) is detected. In addition, it can be observed that the population of spheres ranges from 67% to 84% as *t* spans the 17−88 h interval. Moreover, there is a significant fraction of NPs (10−20%) with triangular profile, which remains invariant over the whole reaction course. On the other hand, the initially negligible population of NRs with AR > 2 (<3%), which slightly increases up to $t = 63$ h (~9%), exhibits a remarkable depletion after irradiating for $t = 88$ h.

The product of syntheses carried at the smallest amount of Ag^+ ions added (*Au_60 series*), is still dominated by nearly isotropic NPs (Figure 1B) that comprise spherical objects and NRs with AR < 2 (>80%). Conversely, the population of anisotropic NPs, composed of triangular prisms and NRs having AR > 2, has now reached <10−20%. The relative fraction of NRs with AR > 2 is very low (1−10% with a maximum at $t = 21$ h). It can be also noted that anisotropic shapes progressively disappear during the irradiation along with a concomitant

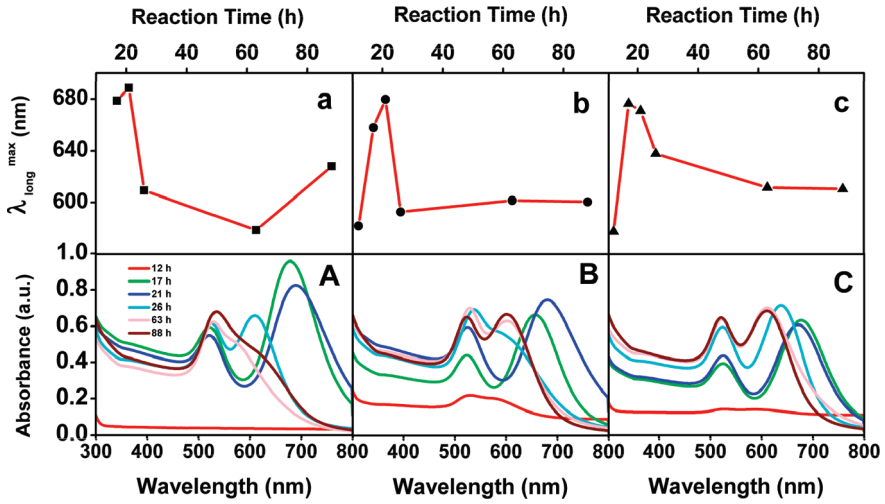

Figure 2. (top panels) Time-dependent shift of longitudinal SPR absorption peak detected for some of the sample series investigated: (a) Au_30, (b) Au_20, and (c) Au_15 (cf. Table 1). (bottom panels) Evolution of the absorption spectrum for the corresponding reaction mixtures during Au NP growth: (A) Au_30, (B) Au_20, and (C) Au_15 series, respectively.

increase in the population of isotropic NPs, which achieves its maximum density at the end of the experiment ($t = 63-88$ h).

Upon increasing the Ag^+ ion amount (Au_30 and Au_20 series), anisotropic NPs become significantly abundant at $17 < t < 21$ h (at which NRs having AR > 2 constitute >60% and >68% of the total population, respectively). On the other hand, this result tends to be reversed for longer reaction times, at which the population of isotropic NPs instead prevails (sphere + spheroids = 80−90% for Au_30 series and 75−85% for Au_20 series; respectively; Figure 1C and D).

A further increase in the Ag^+ loading (Au_15 series) leads to NPs with various shapes (triangles, cubes, and NRs with AR < 2), which cannot be unambiguously discriminated simply by the analysis of the SPR features in the absorption spectra. The population of NRs with AR > 2 reaches its maximum at $t = 21$ h, while further irradiation causes a broadening of the shape distribution (Figure 1E).

Evolution of NP Sizes. In the case of Ag^+-free synthesis (Au_no_Ag series), the mean AR of the NRs reaches its maximum at $t = 21$ h, which is followed by a steady decrease accompanied by a broadening of the AR distribution (Figure S1 in the Supporting Information). At the same time, the mean NR diameter is seen to grow to a little extent, while the NR length instead shows a slight reduction. In other words, it appears that the NR volume maintains, on average, an almost constant value for $t >$ 21 h. It can be noticed that the few NRs detectable (<3%) are very large and distinguished by the highest AR ever observed (in the 3−10 range) in our experiments, although their size distribution is exceedingly broad. The presence of a small amount of Ag^+ ions (Au_60 series) causes a dramatic shrinking in the mean AR (up to <2) although the size distribution appears to be quite narrow. NRs with AR ≥ 2 are revealed as transient species only for $17 < t <$ 21 h (Figure S2 in the Supporting Information). Therefore, the addition of $AgNO_3$ dramatically suppresses NR development. The anisotropic growth seems to be preferred in the $17 < t < 21$ h interval, with the AR approaching its maximum at $t = 21$ h. After that, the aspect ratio decreases very slowly (its value remains almost unchanged until $t = 88$ h). Actually, a simultaneous decrease in both NR diameter and length can be observed, which transcribes into a contraction of the mean NR volume. The average size of nearly spherical NPs increases until $t = 26$ h, after which a size decrease associated with a broadening of the size dispersion is observed.

Similar trends have been observed for syntheses accomplished using proportionally higher Ag^+ loadings in the reaction environment (Au_30, Au_20, and Au_15 series). The average AR of the NRs increases for $17 < t < 21$ h, reaching a maximum value of ~ 2.5 at $t = 21$ h (Au_20 series), and then declining upon prolonged irradiation (Figure S3−S5 in the Supporting Information). Such a NR shortening proceeds along with an enlargement in the NR diameter and a broadening of the related size distribution, while the average NR length tends to decrease as well. As for what regards the sample fraction of nanospheres, the average NP diameter grows up to $t = 26$ h, after which it tends to shrink, while being accompanied by a spreading of the size dispersion. Such findings can be explained by considering the relatively large contribution from spheroidlike NPs (i.e., object of approximately spherical shape) that are generated in the population.

It is worth mentioning that the dimensional and morphological changes observed at $t > 21$ h take place exclusively under UV irradiation. Reaction aliquots withdrawn from the reaction vessel indeed were stable over time when stored in the dark.

Evolution of Absorption Spectra. The time-dependent optical properties of the as-synthesized Au NPs are highlighted in Figure 2. In the case of samples synthesized in the absence of Ag^+ ions and at low Ag^+ content (Au_no_Ag and Au_60 series, respectively), the UV−vis absorption spectra reveal the typical transverse SPR band centered at around 520−540 nm, which is consistent with

the predominance of spherical NPs observed by TEM at all of the reaction times investigated (Figure S6A and B in the Supporting Information). In addition, the absorption features at $t = 7$ h, evidenced by a characteristic broadband in the 390−500 nm range (Figure S7 in the Supporting Information) suggest that Au ion-surfactant complexes are still present in solution,[10] whereas after $t =$ 12 h just a very weak SPR can be appreciated. Accordingly, no Au product can be recovered for $t < 12$ h.

At gradually higher concentration of Ag^+ ions in the growing mixtures (Au_30, Au_20, and Au_15 series, respectively), the absorbance spectra show the longitudinal SPR band centered at 680−700 nm for $t > 17$ h, which is indeed compatible with the existence of anisotropically shaped NPs, like NRs (Figure 2A−C). The spectral position of the maximum (λ_{long}^{max}) of the aforementioned SPR band is observed to red-shift for $17 < t < 21$ h, according to the average NR AR increases observed by size and shape statistical analysis. On the other hand, the blue shift detected in the subsequent period ($t > 63$ h) indicates that the synthesis product tends to be enriched with more isotropic NPs. Regardless of the Ag^+ amount added, the absorption data points out that no significant SPR band are yet visible at $t = 12$ h (Figure 2A−C), which confirms that a considerably long induction period precedes NP nucleation and growth in the surfactant system under investigation.

Elemental Analysis. The chemical composition of the residual reaction mixture (i.e., the supernatant) and of the collected NPs has been evaluated by ICP-AES analysis and expressed in terms of [Au]:[Ag] molar ratio. Irrespective of the initial [Au]:[Ag] molar ratio in the starting mixtures, the time evolution of Au and Ag species concentration in the supernatants is characterized by a sudden decrease in concomitance with the appearance of the SPR band in the absorption spectra (at $t = 17-21$ h; see Figures S8 and S9 in the Supporting Information). Figure 3 reports the time dependence of the chemical composition of the collected Au NPs. It is found that the tiny NPs that are retrieved in the early stages of the growth (at $12 < t < 17$ h; note that, at sizes smaller than 2−3 nm, NPs do not exhibit any clear SPR band, as reported in Figure 2) are far richer in Au (for instance, [Au]:[Ag] = 120:1 is measured for NPs synthesized at a nominal [Au]:[Ag] = 60:1 in the initial reaction mixture). On the other hand, upon further growth ($21 < t < 26$ h), the collected NPs become progressively enriched with Ag (Figure 3). For instance, the sample synthesized at a nominal [Au]:[Ag] value of 20:1 (Au_20 series) and grown for $t = 21$ h (at which NRs with the highest AR are achieved) shows an [Au]:[Ag] ratio (10:1) lower than that expected, thus clearly indicating that such NPs are richer in Ag.

Structural Characterization. *TEM and CBED Analyses*. A comprehensive structural investigation has been carried out by combining TEM imaging and CBED analysis, as reported in Figure 4. NRs grown with or without the assistance of Ag^+ ions have been investigated in order to identify their growth orientation, which

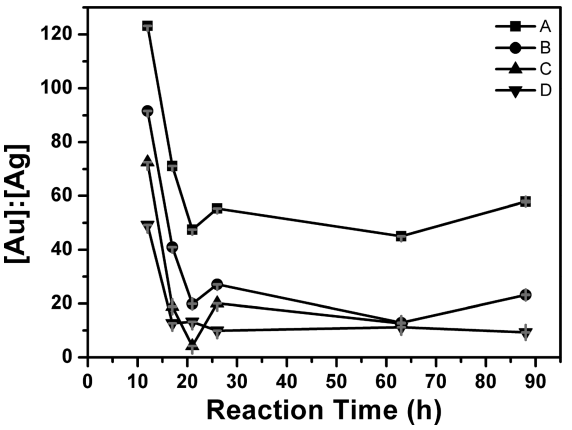

Figure 3. ICP-AES analysis of the chemical composition of the as-prepared Au NPs as a function of the reaction time, expressed in terms of [Au]:[Ag] molar ratio, for the various sample series investigated (cf. Table 1): (A) Au_60; (B) Au_30; (C) Au_20; (D) Au_15. The Ag-free set of samples (Au_no_Ag series) has not been obviously considered due to the absence of silver in the reaction mixture (see also Figure S8 in the Supporting Information).

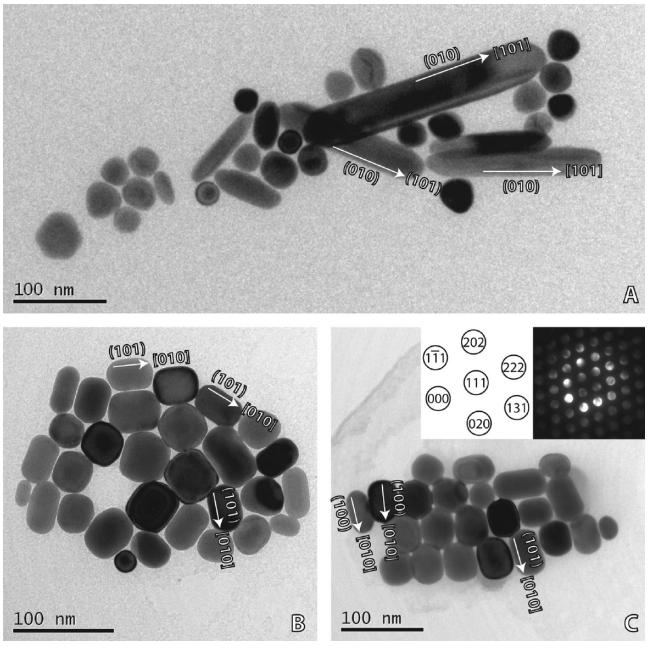

Figure 4. Bright-field TEM images of small groups of Au NRs: (A) NRs prepared in the absence and (B and C) in the presence of Ag^+ ions. Preferred elongation directions and longitudinal side facets are indicated A typical CBED pattern (along with the indexation scheme for fcc gold) relative to a NR down its ⟨110⟩ zone axis, which has been used to determine the structural features of the NPs, is also shown in the inset of panel C.

corresponds to the crystallographic directions along which the face-centered cubic (fcc) Au lattice develop the fastest. Interestingly, the very long NRs prepared in absence of Ag^+ ions are elongated along the ⟨101⟩ direction and expose {010} planes on their longitudinal sides (Figure 4A). On the contrary, irrespective of the nominal Ag^+ ion loading used in the growing mixture, Ag^+-assisted syntheses yield single-crystalline Au NRs that develop along the ⟨010⟩ direction, accordingly exposing either the {101} or {100} facets on the most extended longitudinal sidewalls (Figure 4B and C). These findings

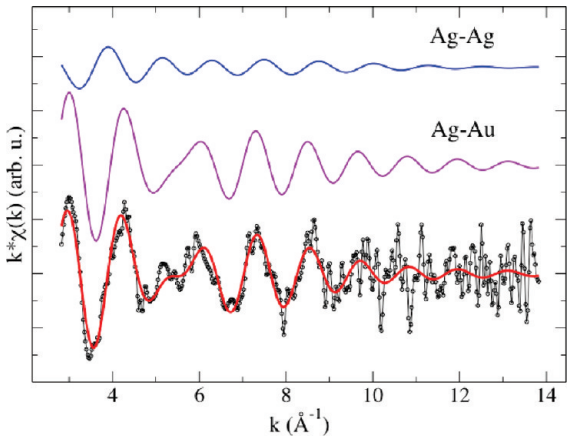

Figure 5. EXAFS experimental data (black circles/line) along with the corresponding best fit (red line) for sample Au_15 irradiated for t = 88 h. The first-shell Ag−Ag (blue) and Ag−Au (violet) signals are shown separately.

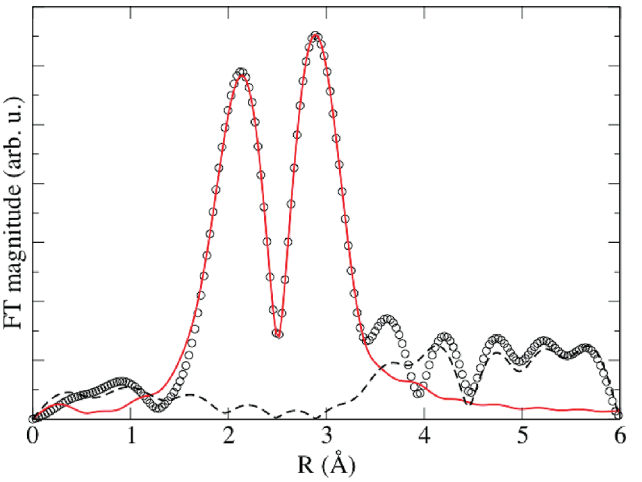

Figure 6. Fourier transform of EXAFS experimental data (circles), the corresponding best fit (red line), and residual (dashes) for sample Au_15 irradiated for t = 26 h.

are significant, in that the involvement of different growth mechanisms, depending on the presence of the Ag^+ ions in solution, can be preliminary drawn. Unfortunately, due to the detection limit of EDS analyses, no Ag has been found in NRs grown in different experimental conditions.

XAS Analysis. In order to clarify the chemical state of Ag, and its role in the NR growth mechanism, XAS measurements have been carried out. As representative cases of study, samples prepared at [Au]:[Ag] of 30 and 15 (Au_30 and Au_15 series) are examined here. The XAS technique probes the local structure around a dilute atomic species (i.e, Ag in this case), providing information on its oxidation state, coordination number (CN), associated bond lengths, and disorder associated with each bond. The foremost advantage of X-ray absorption is that it is limited to the first few coordination shells around the targeted atoms, up to a few angstrom only. Hence, the size, shape, and polydispersity of NPs, the effects of which can be appreciated on a far larger scale (of the order of tens of nanometers), do not affect the XAS spectra to any extent.

The oxidation state of Ag is found to be zero (0) in all the investigated samples. This piece of evidence is proven by both XANES (X-ray absorption near-edge structure) measurements, according to which all of the edge features resemble those of the Ag foil standard, and EXAFS (extended X-ray absorption fine structure) data, which indicate that the nearest neighbors bond lengths are those typical for metal Ag and Ag−Au alloys. As the Au and Ag metal radii are indistinguishable, the interatomic distance values alone cannot be used to discriminate between the Ag−Ag and the Ag−Au correlations. However, because their atomic numbers are different enough, their EXAFS atomic scattering parameters (backscattering amplitude and phase) generate an effective contrast. This is shown in Figure 5, where the EXAFS signals for Ag−Au and Ag−Ag pair correlations are plotted separately. In addition, the presence of both Ag−Ag and Ag−Au correlations in the first coordination shell is evident already in the R-space (i.e., the real space of the interatomic distances) from the appearance of the "first shell doublet"[34] depicted in Figure 6. However, in the Au_30 samples irradiated for t = 21, 63, and 88 h, just a single Ag−Au contribution has been sufficient to reproduce the data, and no further Ag−Ag correlations have been detected.

The main piece of knowledge gained from EXAFS data is that the CN of the first shell around Ag lies in between 3 and 7 in all samples. This is far less than the theoretical CN expected for an Ag atom embedded in a Au NR (CN = 12 for fcc metals) and represents strong proof in favor of the fact that the vast majority of the Ag atoms are located at the near-surface regions of the NPs, as sketched in Figure 7. Contributions due to surface-coordinated solvent and/or surfactant molecules are hardly detectable because of the high thermal disorder.[34]

In the Au_30 sample irradiated for t = 21 h, Ag atoms are 3-fold coordinated by Au atoms. Such an extremely low CN is only compatible with Ag atoms residing on top of a {111} Au surface. The appreciable contraction of the Ag−Au bond length (2.75 vs 2.87 Å) can also be attributed to the strong undercoordination.

In the Au_15 series, in which the Ag^+ ion amount used in the synthesis is higher, some first-shell Ag−Ag neighbors emerge along with Ag−Au correlations. The Ag−Ag bonds, which account for 1−2 nearest neighbors out of 5−7 total coordinating atoms around each Ag atom, most likely arise from flat Ag islands (2−4 atoms wide) lying on the Au surfaces. Again, the hypothesis of Ag atoms deeply buried in the NR interior can be ruled out, since the CN should otherwise be found to increase dramatically. The existence of Ag−Ag islandlike aggregates is more clearly assessed in samples in which NRs prevail in the NP population, regardless of their AR (e.g., in the Au_30 series). In the latter case, a first-shell CN between 5 and 7 is extracted from the EXAFS data fitting, which is compatible with Ag atoms either embedded in or just one atomic layer below the outermost {110} and

(34) Shibata, T.; Bunker, B. A.; Zhang, Z.; Meisel, D.; Vardeman, C. F.; Gezelter, J. D. *J. Am. Chem. Soc.* **2002**, *124*, 11989.

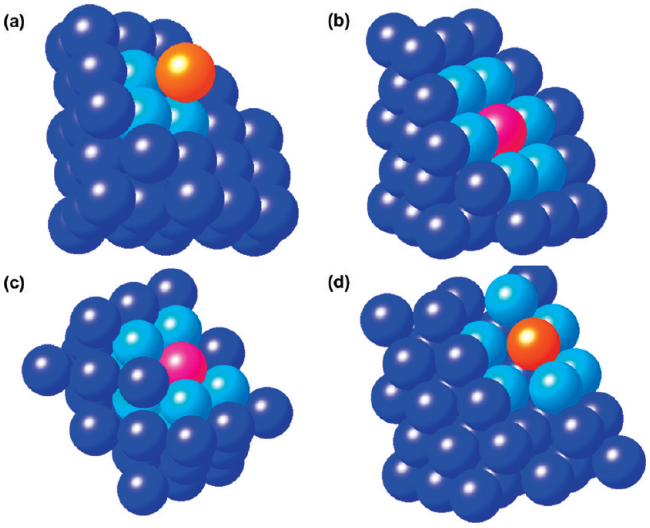

Figure 7. Simulation of possible configurations for Ag atoms embedded in Au NRs at their near-surface regions: (A) Ag atom (orange) on top of a {111} surface of fcc gold. (B) Ag atom (purple) embedded in a {111} surface. (C) Ag atom (purple) embedded in a {100} surface. (D) Ag atom (orange) embedded in a {110} surface. The first shell neighbors are shown in cyan.

{100} facets, or sitting on top of them, or with combination of these configurations (Figure 7). The possibility of a significant incorporation of Ag atoms in near-surface layers of {111} facets, or their adsorption on top of them, can be safely excluded, since the associate CN should otherwise be either 3 or 9. Taken together, the EXAFS data indeed suggest that the deposition of Ag(0) islands occurs preferentially on top of the most developed facets of the NRs, i.e., those corresponding to their longitudinal sidewalls, as identified by CBED/TEM investigations. Such a correlation can be therefore expected to have important implications in the mechanism of anisotropic Au growth.

Discussion

This work has been aimed at gaining a deeper insight into the role of Ag^+ ions in directing the formation of rod-shaped Au NPs in suitable surfactant media by means of a UV-light-driven seedless route. This issue is of particular relevance, since elucidation of the mechanism through which Ag^+ ion additives act as promoters of anisotropic growth is currently an open question also in conventional seed-mediated approaches to Au nanostructures carried out in similar colloidal environments.

The seed-mediated approach involves a two-step procedure. In the beginning, nearly spherical NPs, a few nanometers in size, which are commonly referred to as the "seeds", are independently prepared by chemical reduction of an Au salt. Subsequently, such seeds are used as nucleation centers for catalyzing the growth of Au NRs in a distinct surfactant environment, a process that takes place at a rather fast rate and, hence, is difficult to investigate in detail at different stages of advancement. On the other hand, the one-pot photochemical approach addressed here is advantageous in that both nucleation and growth occur in the same reaction medium quite slowly, which allows a straightforward monitoring of NP growth by both spectroscopic and structural investigation tools.

The mechanism underlying the formation of Au(0) from Au(III) has so far been mostly unclear. For instance, the chemical nature of the actual Au precursors in aqueous $HAuCl_4$-loaded surfactant mixtures is still under debate. Some reports have proposed the formation of an $AuCl_4^-$–CTAB complex,[18] whereas other studies have suggested that Br^- ions, which are present in solution as the CTAB counterions, can replace Cl^- ligands in the $AuCl_4^-$ complex, leading to the formation of $AuBr_4^-$ species.[10,32] In order to clarify this issue, we have analyzed the absorbance spectra of $AuCl_4^-$ solution following the addition of KBr or CTAB, in the presence of both Br^- ions and surfactants. By comparing the spectra recorded, it appears plausible that such substitution of Br^- for Cl^- may occur also in our experimental conditions (Figure S10 in the Supporting Information). Therefore, in agreement with previous reports,[10,32] the actual Au precursor in our experimental conditions could be safely considered to be $AuBr_4^-$ rather than $AuCl_4^-$.

In the whole set of experiments, the formation of Au NPs is observed only after 7–12 h of irradiation. The occurrence of such an induction period seems to be independent of the Ag^+ ion amount, although a further slightly delayed nucleation has been observed for syntheses carried out at a nominal [Au]:[Ag] ratio lower than 30. As a matter of fact, only in the absorption spectra of samples prepared without Ag^+ and at [Au]:[Ag] = 60 (Au_no_Ag and Au_60 series, respectively) a weak SPR feature can be observed after t = 12 h (cf. Figure 2 and Figure S6 in the Supporting Information).

It deserves noting that no Au NPs have been obtained in the experiments carried out in the absence of acetone, thus indicating that in our experimental conditions Au(III) species reduction is promoted by acetone, while UV light alone does not suffice to cause Au NP nucleation.[32]

The photophysics of acetone has been extensively studied.[35–38] Under UV irradiation ketyl radicals are generated via excitation of acetone and subsequent hydrogen atom abstraction from RH:

$$(CH_3)_2CO + h\nu \rightarrow (CH_3)_2CO^* \quad (1)$$

$$(CH_3)_2CO^* + RH \rightarrow (CH_3)_2{}^{\bullet}COH + {}^{\bullet}R \quad (2)$$

where RH and $^{\bullet}$R denote the CTAB and alkyl radical generated from CTAB, respectively.[32] Such radicals are known to be strongly reducing agents and could be thus responsible for the reduction of Au(III) and Ag(I) ions.[39]

It has been proposed that Au(III) can be reduced to Au(I) via a multiple-step reduction process involving the

(35) Kasama, K.; Takematsu, A.; Arai, S. *J. Phys. Chem.* **1982**, *86*, 2420.
(36) Borkman, R. F.; Kearns, D. R. *J. Chem. Phys.* **1966**, *44*, 945.
(37) Haas, Y. *Photochem. Photobiol. Sci.* **2004**, *3*, 6.
(38) Vaish, S. P.; McAlpine, R. D.; Cocivera, M. *J. Am. Chem. Soc.* **1974**, *96*, 1683.
(39) Henglein, A. *Chem. Mater.* **1998**, *10*, 444.

disproportionation of unstable Au(II) species (eqs 3 and 4).[40] Au(I) could be stabilized by CTAB, which could, in turn, allow the accumulation of Au(I) species up to a "critical concentration" at which a fast nucleation is induced (eqs 5 and 6):[10,18,32]

$$Au^{3+} + (CH_3)_2{}^{\bullet}COH \rightarrow Au^{2+} \quad (3)$$

$$2Au^{2+} \rightarrow Au^{+} + Au^{3+} \quad (4)$$

$$Au^{+} + (CH_3)_2{}^{\bullet}COH \rightarrow Au^{0} + (CH_3)_2CO + H^{+} \quad (5)$$

$$nAu^{0} \rightarrow Au_n(NPs) \quad (6)$$

Actually, prior to the appearance of the SPR band (at $t = 17$ h), the solution color turns from pale yellow ($t = 0-7$ h) to colorless ($t = 12$ h), which reflects the formation of Au(I)−CTAB complexes upon reduction of their Au(III)−CTAB parents.[18,29,41] In addition, the hypothesis, according to which the nucleation burst requires the crossing of a sufficiently high Au(I) concentration threshold to be triggered, is consistent with the detection of aforementioned induction time, the end of which is marked by the emergence of SPR absorption and by a sudden Au concentration decrease in the reaction supernatants (at $t = 17-21$ h; see also Figure 2 and Figures S6, S8, and S9 in the Supporting Information).

In previous studies on the Ag^+-ion-assisted photochemical synthesis of Au NRs, it has been assumed that an Au−Ag alloy formed in the early stages of NP formation. However, we do not have any experimental proof to support such a postulation. In fact, the chemical composition of the Au NPs collected in the 7−21 h interval (Figure 3) and the absence of Ag atoms deeply embedded in the Au lattice (as demonstrated by EXAFS measurements) suggest that Ag^+ ions should not be reduced at this stage. Nevertheless, the induction time appears to become progressively longer (albeit to a little extent) as the Ag^+ loading is increased (see the Au_30, Au-20, and Au_15 series, Figure 2, and Figure S6 in the Supporting Information). A similar delay in the nucleation and growth of NPs has been already observed in the case of Ag^+-assisted seed-mediated approach.[31] Such behavior could be accounted for by invoking a competitive reduction of Ag(I) and Au(III) precursors involving the presence of an Au(I) intermediate. As a matter of fact, the reduction of Au(III) to Au (0) in a seed-mediated approach assisted by $AgNO_3$ has recently been monitored by cyclic voltammetric measurements demonstrating the presence of Au(I) intermediates.[42]

Taking into account the lack of Ag−Au alloy experimental evidence, it can be assumed that Au(I) is first reduced to Au(0) under UV light according to eq 5, while Ag^+ reduction could be expected to take place more easily via uptake of electrons at the surface of the Au seeds initially nucleated,[31] which would lead to tiny Ag(0) clusters and/or islands adsorbed thereon. On the other hand, Ag(0) could be reoxidized to Ag^+ in the presence of Au(I) species,[43,44] thus allowing the growth of Au NPs that do not incorporate Ag deeply in the Au lattice. Such Ag reduction/oxidation dynamics could account for the lack of evidence for the formation of Ag−Au alloyed NPs during NR growth.

Under the experimental conditions used by us, the concentration of Ag(0) achieved at the surface of the as-synthesized NPs is apparently too low to be appreciated via EDS. Although some authors have proposed the formation of AgBr that could adsorb onto the Au NP surface,[32] nevertheless our EXAFS data have not revealed any Ag−Br correlation or the presence of Ag(I) species on the Au NP product. As a matter of fact, only negligible contamination from colloidal AgBr should possibly be expected to be attained in solution ($k_{sp}(AgBr) = 5.35 \times 10^{-13}$).[31]

The most crucial issue in Au NR synthesis is how to guarantee the production of NRs in far larger yield over more isotropic shapes (e.g., nanospheres, spheroids). Previous works on the seed-mediated approach have suggested that the selection of certain additives can cause elongation of the micelles and/or drive enlargement of their size,[45] which could thus offer larger nanoreactors for templating the growth of more anisotropic Au NPs with improved NR yield.[16,29,45,46] For instance, small amounts of cyclohexane and other alkanes (cyclooctane, cyclodecane, trans-decalin, *n*-hexane, 2,3-dimethylbutane, or adamantine) can drive CTAB micelles to take rodlike shape.[47] Nevertheless, in our experiments, Ag^+-free syntheses performed with controlled additions of extra cyclohexane provided only a minor fraction of NRs with a very broad size distribution, from which it can be inferred that the formation of a rodlike micellar template is not the most influential factor accounting for anisotropic growth of Au NPs. Rather, the presence of Ag^+ at a suitable concentration appears to play a crucial role in controlling the NP shape and the NR yield. Indeed, upon increasing the Ag^+ content in the growing environment (cf. Table 1 and Figure 1), the population of NRs with AR >2 observed at a fixed irradiation time (e.g., at $t =$ 21 h) increases from ~11% to ~68%, respectively. On the other hand, an Ag^+ excess prevents the formation of NRs having AR > 2 (e.g., only 36% in the series prepared at [Au]:[Ag] = 15). At the same time, the population of triangles and cubes undergoes a dramatic drop. For

(40) Meyre, M.-E.; Treguer-Delapierre, M.; Faure, C. *Langmuir* **2008**, *24*, 4421.
(41) Lin, Z.-j.; Chen, X.-m.; Cai, Z.-m.; Oyama, M.; Chen, X.; Wang, X.-r. *Cryst. Growth Des.* **2008**, *8*, 863.
(42) Seo, S.; Wang, X.; Murray, D. *Ionics* **2009**, *15*, 67.
(43) Chen, H. M.; Hsin, C. F.; Liu, R.-S.; Lee, J.-F.; Jang, L.-Y. *J. Phys. Chem. C* **2007**, *111*, 5909.
(44) Xu, Z.-C.; Shen, C.-M.; Xiao, C.-W.; Yang, T.-Z.; Zhang, H.-R.; Li, J.-Q.; Li, H.-L.; Gao, H.-J. *Nanotechnology* **2007**, *18*, 115608.
(45) Jana, N. R.; Gearheart, L.; Murphy, C. J. *Adv. Mater.* **2001**, *13*, 1389.
(46) Busbee, B. D.; Obare, S. O.; Murphy, C. J. *Adv. Mater.* **2003**, *15*, 414.
(47) Tornblom, M.; Henriksson, U. *J. Phys. Chem. B* **1997**, *101*, 6028.

instance, in the samples synthesized at [Au]:[Ag] ratio of 30, 20, and 15, the total population of spheres and NRs ranges from 90% to 97%, respectively. Taken together, these facts imply that Ag^+ ions are capable to prevent NP growth in some crystallographic directions of their fcc lattice.

Importantly, the high-AR NRs that have occasionally been observed in the Ag^+-free samples grow along the ⟨101⟩ direction, exposing {010} planes along the longitudinal sidewalls. On the contrary, Au NRs prepared in the presence of Ag^+ (Figure 4B and C) develop along the ⟨010⟩ direction, and are longitudinally enclosed by either {101} or {100} planes. It seems thus reasonable to conclude that Ag^+-assisted synthesis, including both those achieved photochemically[26] (like in this study) or by seeding in CTAB media,[31] result in Au NRs that are structurally similar to those grown via electrochemical methods.[15] As opposed, NRs produced photochemically without Ag^+ assistance resemble those reported for other seed-mediated CTAB methods.[43,48]

EXAFS data have shown that the presence of Ag−Ag correlation, due to surface-adhering Ag islands, is more frequent in samples with high prevalence of NRs in the NP population. A preference for Ag atoms to be embedded in the near-surface atomic layers and/or on top of {110} and {100} facets can be therefore assumed, which would stabilize the latter, thereby restricting lattice development in the relevant crystallographic directions associated. This explanation is in good agreement with the particular NR elongation that has most frequently been identified by CBED/TEM investigations. The preferential adsorption of Ag(0) clusters on the aforementioned facets can be explained by considering that, in a fcc structure, unpassivated {110} facets are characterized by higher surface energy than that of {111} and {100} facets[49] due to their open configuration (Figure 7). It follows that an Ag monolayer could be preferably adsorbed or deposited onto {110} facets as a convenient means of decreasing their surface energy. Ag monolayers or islands over {110} facets can be ultimately regarded as acting as a strongly binding "surfactant" layer that protects such surfaces against fast growth upon accommodation of additional material from solution precursor species.

A similar model based on facet-preferential Ag adsorption has recently been invoked to explain anisotropic growth of seeded Au NRs through a mechanism of underpotential deposition (UPD) of Ag^+ ions.[31,50,51] UPD is a phenomenon occurring when a metal submonolayer or monolayer is deposited onto the surface of a different metal. It has been observed that, when a metal working electrode is slowly cathodically polarized, ions of a second, less noble metal can be deposited onto it, forming an extremely thin film. The deposition of the first and, sometimes, of the second monolayer, occurs at a potential significantly less negative than that required for the deposition of the corresponding bulk metal. The chemical activity of the adlayer can be smaller than the bulk value (unity), if only a submonolayer with very low coverage is formed.[52] In addition, the chemical potential of the adsorbate is lower than the value associated to its bulk counterpart. On the basis of the theory of Kolb et al.,[53] UPD can occur only when the work function of the bulk metal of which the adlayer is made is lower than the work function of the bulk metal of which the substrate electrode is composed. The work function of Ag is lower than that of Au by more than 0.5 eV; therefore, the UPD of Ag can be expected to take place over Au. For these metals, the work function differences are 0.83, 0.85, and 0.57 eV for their {100}, {110}, and {111} facets, respectively. The latter should clearly exhibit a much lower UPD shift for Ag^+ than the other two plane families. However, when comparing the {100} and {110} planes, it should be more carefully considered that {110} facets possess a more open surface structure (i.e., characterized by a higher number of dangling bonds) than that characterizing {100} facets. On the basis of the all the arguments above, the UPD shifts of Ag^+ on Au surfaces can be expected to be in the order: {110} > {100} > {111}, thus accounting for the preferential adsorption of Ag onto {110} and {100} facets postulated earlier.[31,50,52]

It can be also proposed that the Ag layer can be reoxidized (e.g., by Au(I) species)[43,44] and replaced by Au ions in the solution. On average, the process of Ag deposition/oxidation can be expected to slow down the growth rate of Au along the ⟨110⟩ directions. By comparison, {111} or {100} facets[19,54] (corresponding to the NR apexes) could be either only partially covered by Ag or left completely uncovered, which would make them grow much faster, ultimately resulting in NRs elongated along the ⟨100⟩ direction. The ratio of the ⟨100⟩ to ⟨110⟩ development rate has been found to be tunable by varying the Ag^+ ion concentration, which explains why the latter dictates the range of AR values with which the NRs can be ultimately accessed.[31]

At longer irradiation times, the overall concentration of Au species (i.e., [Au(III)] + [Au(I)]) in the solution becomes negligible (see ICP-AES data). In such circumstances, the NP size and shape evolution can still occur, however via dissolution of the most unstable NPs. This ripening process, which requires UV irradiation to be activated (the samples stored in the dark do not, in fact, undergo any change), can account for the simultaneous NR shortening and increase in the relative fraction of spheres and spheroids in the NP population. In this

(48) Johnson, C. J.; Dujardin, E.; Davis, S. A.; Murphy, C. J.; Mann, S. *J. Mater. Chem.* **2002**, *12*, 1765.
(49) Wang, Z. L.; Gao, R. P.; Nikoobakht, B.; El-Sayed, M. A. *J. Phys. Chem. B* **2000**, *104*, 5417.
(50) Grzelczak, M.; Perez-Juste, J.; Rodriguez-Gonzalez, B.; Liz-Marzan, L. M. *J. Mater. Chem.* **2006**, *16*, 3946.
(51) Chen, H. M.; Liu, R.-S.; Tsai, D. P. *Cryst. Growth Des.* **2009**, *9*, 2079.
(52) Grzelczak, M.; Perez-Juste, J.; Mulvaney, P.; Liz-Marzan, L. M. *Chem. Soc. Rev.* **2008**, *37*, 1783.
(53) Kolb, D. M. *Advances in electrochemistry and electrochemical engineering*; Wiley: New York, 1978; Vol. *11*.
(54) Seo, D.; Park, J. H.; Jung, J.; Park, S. M.; Ryu, S.; Kwak, J.; Song, H. *J. Phys. Chem. C* **2009**, *113*, 3449.

Scheme 1. Proposed Reaction Mechanism for the Ag^+-Ion-Mediated Formation of Au NRs[a]

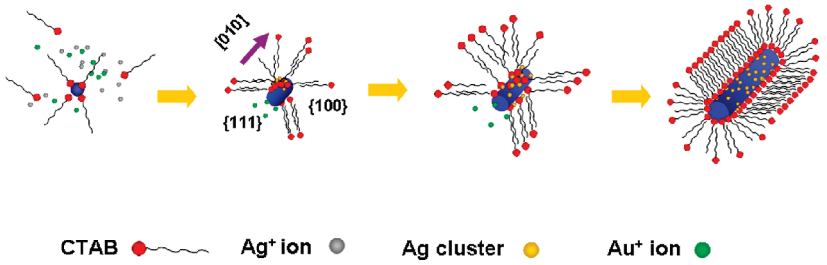

[a] Growth is allowed to proceed preferentially along the ⟨010⟩ direction.

regime, the less protected {100} facets can be more prone to dissolve, leading to a reduction in average AR values. On the other hand, the Ag(0) and surfactant-stabilized {110} facets can continue their growth, albeit at a slower rate, in agreement with the experimentally determined evolution of the NP geometric parameters.[26]

Summary and Conclusions

The Ag^+- ion-mediated photochemical synthesis of water-soluble Au NPs in a micellar template has been investigated as a function of Ag^+ ion amount and of the reaction time. The reaction course has been monitored by optical, structural, and size-morphological monitoring of the evolving NPs. EXAFS experiments have demonstrated, for the first time, the fate of Ag^+ ions and their chemical state and environment in the final product. The whole ensemble of results, gathered from judicious combination of complementary investigative tools, allows us to propose reasonable mechanistic pathways for the formation of anisotropically shaped Au NPs, sketched in Scheme 1.

The occurrence of an induction period prior to the NP nucleation, accompanied by distinguished spectral changes, supports the hypothesis that the first reaction step involves the reduction of Au(III) to Au(I). The invariant presence of Au species in solution during the entire induction period is consistent with CTAB-driven stabilization of Au(I) species, which are therefore allowed to accumulate until the critical supersaturation threshold is reached. From this point on, NP shape evolution can be easily followed by complementary TEM and SPR absorption measurements. During growth, Ag(0) adsorbs onto {100} and {110} facets, with the average crystal development being preferred along the ⟨010⟩ direction of the fcc lattice (see Figure S11 in the Supporting Information).

The present study, providing a rationale for the anisotropic growth of Au NPs in surfactant mixtures by a photochemical approach, could be useful to the design of more controllable synthetic routes to anisotropic Au nanostructures, which could be extended to other metal systems.

Acknowledgment. This work has been partially supported by the EC-funded project NaPa (Contract no. NMP4-CT-2003-500120), by COST D43 "Action On Colloid And Interface Chemistry For Nanotechnology" and by the MIUR SINERGY programme (FIRBRBNE03S7XZ). The authors also gratefully thank the staff of the beamline BM8 at ESRF (Grenoble, France) for assistance during EXAFS measurements, Dr. Giuseppe Mascolo and Dr. Giuseppe Ciccarella for ICP-AES analyses and Benedetta Antonazzo for TEM measurements performed by Jeol JEM 1011 microscope.

Supporting Information Available: Additional absorbance spectra, ICP-AES elemental data, size and size distribution statistical data, and SAXS measurements. This material is available free of charge via the Internet at http://pubs.acs.org.